

FDA Beampattern Characteristics With Considering Time-Range Relations

Wenkai Jia, Wen-Qin Wang, *Senior Member, IEEE*, Shungsheng Zhang, Zhi Zheng,

Abstract—Existing investigations show that frequency diverse array (FDA) will produce angle-range-dependent and time-variant transmit beampattern, but the relations between time and range and their characteristics still are not fully investigated. In order to fully exploit the time and range dependent characteristics of FDA transmit beampattern and address the effects of FDA frequency offsets, we systematically reformulate the FDA antenna and system model with specific time-range relation consideration. Two FDA transmit beampatterns, namely, instantaneous and integral ones, are derived. Accordingly, the FDA time and range dependent characteristics together with the comparisons to conventional phased-array and co-located multiple-input multiple-output (MIMO) antennas are analyzed. Both theoretical analysis and simulation results reveal that the FDA time-range dependent characteristics actually can be regarded as auto-scanning capability, which may provide many promising applications.

Index Terms—Frequency diverse array (FDA), FDA antenna, transmit beampattern, time-variant beampattern, beampattern synthesis, auto-scanning antenna, range-time relations.

I. INTRODUCTION

THE concept of frequency diverse array (FDA) was first proposed in 2006 [1], [2] and patented by Wicks and Antonik [3], [4]. Compared to phased-array, FDA employs different carrier frequencies across the array elements to generate the transmit beampattern as a function of the angle, range and even time [5]–[8]. The fusion of frequency diversity and spatial diversity provides FDA with broad application prospects [9]–[13].

As the standard FDA usually produces an S-shaped beampattern in the angle-range plane [14], logarithmic [15], time-modulated [16], [17], random [18] and optimized [19] frequency offsets (FOs) were suggested to decouple the beampattern. Combining co-located multiple-input multiple-output (MIMO) with waveform diversity [20], distributed MIMO with spatial diversity [21] and FDA, a focused transmit beampattern was synthesized by optimizing the transmitted baseband complex waveform [22]. Furthermore, to obtain dot-shaped time-invariant beampattern, alternating direction method of multipliers (ADMM) algorithm was adopted to design the transmitted weight matrix in [23]. On the other hand, multiple methods have been proposed to explore the angle-range-dependent property of FDA transmit beampattern, such as

dual-pulse FDA [24], FDA-MIMO [25] and FDA subarrays [26]. Basit *et al* [27] studied the use of FDA with nonlinearly progressive frequency offsets for joint radar and communication functionalities. Xu *et al.* proposed an FDA strategy for identifying and suppressing deceptive mainlobe interference [28] and suppressing range-ambiguous clutter, which show better performance than phased-array [29]. Additionally, FDA for low probability of intercept (LPI) transmit beamforming [14], [30] and secure communications [31] also were reported.

Since the range-angle coupling and time-variant beampattern characteristics are essence of FDA antenna that is distinct from conventional phased-array and MIMO antennas, it is more meaningful to effectively utilize the time variance to improve the application performance rather than to decouple the beampattern. This is not only that its time-variant property cannot be adequately suppressed at all, but the obtained pseudo-static or focused FDA will lose its advantage in the competition with phased-array and MIMO antennas. FDA transmit beampattern time variance was analyzed in [32] and [33], but the time-range relations and the effects of frequency offsets still are not thoroughly studied.

In this paper, we reformulate the FDA antenna system model and reinterpret the time and range dependent characteristics of the FDA transmit beampattern, together with extensive comparisons with conventional phased-array and MIMO antennas. Our main contributions are listed as follows:

- 1) With the exact understanding about the time-range relations, the accurate models of time-invariant beampatterns for FDA are presented. Moreover, we reinterpret the time and range dependent characteristics of FDA transmit beampattern, which proves the auto-scanning property.
- 2) The instantaneous FDA transmit beampattern model (FITB) is formulated with time variance consideration, and a frequency offset design scheme for realizing FDA multi-beam transmission is given, which shows equivalence to conventional phased-array.
- 3) The integral FDA transmit beampattern model (FGTB) is derived and the corresponding effects of frequency offsets are analyzed. It is shown that, if waveform optimization is further employed, the equivalence to a co-located MIMO beampattern can be achieved.

The remaining sections are organized as follows. Section II presents the FDA antenna model and reinterprets the characteristics of the FDA transmit beampattern with specific time-range relations consideration. In Section III, the FITB is formulated with time variance consideration and the design of the initial main lobe direction is discussed. In Section IV, the

This work was supported by National Natural Science Foundation of China 62171092 and Sichuan Science and Technology Program under grant 2018RZ0141. (Corresponding author: Wen-Qin Wang)

The authors are with School of Information and Communication Engineering, University of Electronic Science and Technology of China, Chengdu, 611731, P. R. China. (email: mrwenkaij@126.com; wqwang@uestc.edu.cn; zhangss@uestc.edu.cn; zz@uestc.edu.cn).

influence of nonlinear and time-modulated FOs on FITB is evaluated and a frequency offset design scheme for realizing FDA multi-beam transmission is given. Next, the FGTB model is derived in Section V, followed by corresponding FO effect analysis and comparison with the co-located MIMO antennas. Finally, conclusions are drawn in Section VI.

II. SIGNAL MODEL

Consider a standard uniform linear M -element FDA. The transmit carrier frequency for the m th element is

$$f_m = f_c + m\Delta f, \quad m = 0, 1, \dots, M-1 \quad (1)$$

where f_c and Δf denote the reference carrier frequency and FO, respectively. The transmitted pulsed-FDA signal can then be expressed as

$$x(t) = \sum_{m=0}^{M-1} w_m^* \phi(t) e^{j2\pi(f_c + m\Delta f)t}, \quad t \in [0, T_p] \quad (2)$$

where w_m is the transmitted weight of the m th element and $\phi(t)$ is the transmitted baseband complex waveform with unit energy, namely, $\int_{T_p} \phi(t) \phi^*(t) dt = 1$, where T_p and $*$ are the pulse duration and conjugate operator, respectively.

The synthesized signal arriving at a given far-field point target with the range-angle pair (r_t, θ) (the target slant range r_t takes the first element as the reference) can be written as

$$y(t) = x\left(t - \frac{r_m}{c}\right) =$$

$$\sum_{m=0}^{M-1} w_m^* \phi\left(t - \frac{r_m}{c}\right) e^{j2\pi(f_c + m\Delta f)\left(t - \frac{r_m}{c}\right)}, \quad t \in \left[\frac{r_t}{c}, \frac{r_t}{c} + T_p\right] \quad (3)$$

where $r_m = r_t - md \sin \theta$ and c denote the slant range from the m th element to the target with d being the inter-element spacing and speed of light, respectively.

Considering the narrow-band assumption

$$\frac{Md}{c} \ll \frac{1}{B_{\phi(t)}} \quad (4)$$

with $B_{\phi(t)}$ being the bandwidth of the transmitted baseband complex waveform $\phi(t)$, it holds that $\phi\left(t - \frac{r_m}{c}\right) \approx \phi\left(t - \frac{r_t}{c}\right)$. Then (3) can be approximately expressed as

$$y(t) \approx \sum_{m=0}^{M-1} w_m^* \phi\left(t - \frac{r_t}{c}\right) e^{j2\pi(f_c + m\Delta f)\left(t - \frac{r_t - md \sin \theta}{c}\right)}, \quad t \in \left[\frac{r_t}{c}, \frac{r_t}{c} + T_p\right]. \quad (5)$$

The value range of the time variable t is often neglected in the FDA signal model associated with the FDA transmit beampattern in the FDA literature [19], [23], [34]. In order to fully exploit the FDA beampattern characteristics, we reformulate the FDA transmitted signal model with the time-range relation consideration. We rewrite (5) as:

$$\begin{aligned} r(t') &= \phi(t') e^{j2\pi f_c t'} \sum_{m=0}^{M-1} w_m^* e^{j2\pi m \Delta f t'} e^{j2\pi(f_c + m\Delta f) \frac{md \sin \theta}{c}} \\ &= \phi(t') e^{j2\pi f_c t'} \sum_{m=0}^{M-1} w_m^* e^{j2\pi m \Delta f t'} e^{j2\pi \frac{f_c}{c} md \sin \theta} e^{j2\pi \Delta f \frac{m^2 d \sin \theta}{c}} \\ &= \phi(t') e^{j2\pi f_c t'} \mathbf{w}^H [\alpha_T(t') * \alpha_\theta(\theta) * \alpha_{\Delta f}(\theta)] \\ &\quad , t' \in [0, T_p] \end{aligned} \quad (6)$$

where

- $\mathbf{w} = [w_0 \ w_1 \ \dots \ w_{M-1}]^T$ denotes transmitted weigh vector with T being the transpose operator;
- $\alpha_T(t') = [1 \ e^{j2\pi \Delta f t'} \ \dots \ e^{j2\pi(M-1)\Delta f t'}]^T$,
 $\alpha_\theta(\theta) = [1 \ e^{j2\pi \frac{f_c}{c} d \sin \theta} \ \dots \ e^{j2\pi \frac{f_c}{c} (M-1)d \sin \theta}]^T$,
 $\alpha_{\Delta f}(\theta) = [1 \ e^{j2\pi \Delta f \frac{d \sin \theta}{c}} \ \dots \ e^{j2\pi \Delta f \frac{(M-1)^2 d \sin \theta}{c}}]^T$;
- H and $*$ denote the conjugate transpose operator and Hadamard operator, respectively.

In (6), a variable substitution $t' \leftarrow t - \frac{r_t}{c}$ is used. It must be emphasized that the time uniqueness should be guaranteed in signal modeling. For given target range parameters, the transmit delay is a determined constant, so the only changing part is the time variable t .

Similarity, define the FDA array factor as [35]

$$AF_{\text{FDA}}(t, \theta) = \sum_{m=0}^{M-1} e^{j\gamma_{\text{FDA}}} = \alpha_T^T(t) [\alpha_\theta(\theta) * \alpha_{\Delta f}(\theta)] \quad (7)$$

where $\gamma_{\text{FDA}} = 2\pi \left(m\Delta f t + \frac{f_c m d_T \sin \theta}{c} + m^2 \frac{\Delta f d_T \sin \theta}{c} \right)$ represents the phase difference between the signal transmitted by the m th element and the reference element. In order to obtain the analytic result of (7), we do the following approximation:

$$e^{j2\pi m^2 \Delta f \frac{d \sin \theta}{c}} \approx e^{j2\pi m \Delta f \frac{d \sin \theta}{c}}, \quad m = 0, 1, \dots, M-1. \quad (8)$$

Then, we have

$$AF_{\text{FDA}}(t, \theta) \approx \left| \frac{\sin \left[M\pi \left(\Delta f t + \frac{f_c d \sin \theta}{c} + \frac{\Delta f d \sin \theta}{c} \right) \right]}{\sin \left[\pi \left(\Delta f t + \frac{f_c d \sin \theta}{c} + \frac{\Delta f d \sin \theta}{c} \right) \right]} \right|, \quad t \in [0, T_p]. \quad (9)$$

It is noted from (9) that the FDA array factor is angle-time-dependent within the pulse duration, which exhibits a considerable difference from the phased-array. Since the FDA array factor in (9) is time-variant, we call it FDA instantaneous or time-invariant transmit beampattern (FITB). But the range-dependent property is certainly not available in the FITB.

In the FDA literature [35]–[39], the FDA array factor is often expressed as

$$AF_{\text{FDA}} \approx \left| \frac{\sin \left[M\pi \left(\Delta f t - \Delta f \frac{r_t}{c} + \frac{f_c d \sin \theta}{c} + \frac{\Delta f d \sin \theta}{c} \right) \right]}{\sin \left[\pi \left(\Delta f t - \Delta f \frac{r_t}{c} + \frac{f_c d \sin \theta}{c} + \frac{\Delta f d \sin \theta}{c} \right) \right]} \right| \quad (10)$$

And $t = 0$ is chosen to analyze the instantaneous characteristics of FDA array factor [19]. In this case, the authors concluded that the FDA array factor is time-range-angle-dependent [23], [40]. However, the range-dependent theory of FDA array factor was challenged by the consideration of the Huygens-Fresnel principle [41]. Since the time variable t belongs to $t \in \left[\frac{r_t}{c}, \frac{r_t}{c} + T_p\right]$, the conclusion of the instantaneous FDA array factor is not convincing. Therefore, the FDA characteristics still have not been fully explored in the literature. Nevertheless, it is stated from (9) and (10) that FDA characteristics can be well exploited by analyzing the relation between time and range variables.

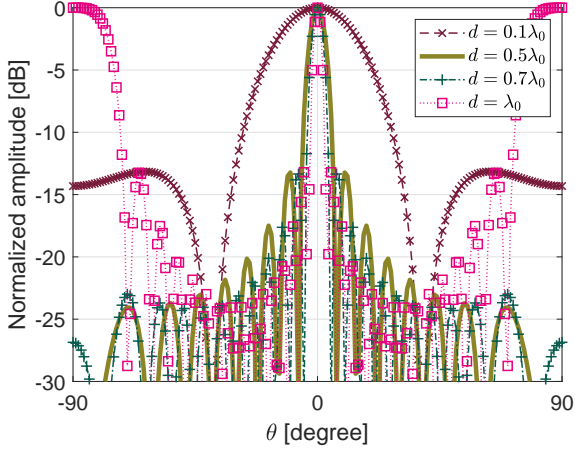


Fig. 1. Zero-time cut of the FITB (9).

III. FDA TIME-INVARIANT TRANSMIT BEAMPATTERN CHARACTERISTICS

A. Zero-time Cut

Let $t = 0$ in (9), the zero-time profile of FITB can be written as

$$AF_{\text{FDA}}(0, \theta) \approx \left| \frac{\sin \left[M\pi \left(\frac{f_c d \sin \theta}{c} + \frac{\Delta f d \sin \theta}{c} \right) \right]}{\sin \left[\pi \left(\frac{f_c d \sin \theta}{c} + \frac{\Delta f d \sin \theta}{c} \right) \right]} \right| \quad (11)$$

It can be interpreted as the FDA beampattern in the azimuth dimension at the initial time. We then we have

- 1) The approximate first null beamwidth (FNBW) is (consider the FO is much smaller than the reference carrier frequency, i.e., $\Delta f \ll f_c$)

$$\Delta \theta = \sin^{-1} \left(\frac{c}{f_c M d} \right), \quad (12)$$

- 2) The beampattern peak is periodic located at

$$\theta_{\text{PEAK}} = \sin^{-1} \left(k \frac{c}{f_c d t} \right), \quad k \in \mathbb{Z} \quad (13)$$

where \mathbb{Z} denote the integer set.

Fig. 1 shows the zero-time cut of the FITB, where $M = 16$, $f_c = 10 \text{ GHz}$ and $\Delta f = 100 \text{ Hz}$ are assumed. It is seen that the larger the inter-element spacing d , the narrower the beamwidth is. If d exceeds half the reference wavelength $\lambda_0 = \frac{c}{f_c + M\Delta f}$, the grating lobes will appear around $\pm 90^\circ$.

B. Time-Variant Property

According to (9), FITB has peaks at the locations satisfying

$$\Delta f t + \frac{f_c d \sin \theta}{c} + \frac{\Delta f d \sin \theta}{c} = k, \quad k \in \mathbb{Z}. \quad (14)$$

The beam at time t steers to

$$\theta = \sin^{-1} \left(\frac{ck - c\Delta f t}{f_c d + \Delta f d} \right). \quad (15)$$

Besides, there are series of angle-time pairs satisfying (14), producing a complex energy distribution within the pulse duration.

Suppose the FITB is oriented to $\hat{\theta}_1$ and $\hat{\theta}_2$ at time t_1 and t_2 , respectively. Then we have

$$\sin \hat{\theta}_1 - \sin \hat{\theta}_2 = \frac{c\Delta f (t_2 - t_1)}{(f_c + \Delta f) d}. \quad (16)$$

Derivating both sides of (15) with respect to t yields the spatial scanning speed of the FITB

$$\begin{aligned} \frac{d\theta}{dt} &= -\frac{c\Delta f}{(f_c + \Delta f) d \cos \theta} \quad d = \frac{\lambda_0}{2} = \frac{c}{2[f_c + (M-1)\Delta f]} \\ &\quad - \frac{2\Delta f [f_c + (M-1)\Delta f]}{(f_c + \Delta f) \cos \theta} \approx -\frac{2\Delta f}{\cos \theta}. \end{aligned} \quad (17)$$

Observing (16) and (17), we conclude that

- 1) Different from phased-array where electronic phase shifters control the beam main lobe direction, FDA can scan the observed airspace automatically. The main lobe direction of FDA beam changes continuously within the pulse duration, and the beam coverage is

$$\begin{aligned} \Delta \theta_{T_p} &= \frac{c\Delta f T_p}{(f_c + \Delta f) d} = \\ &\quad \frac{\Delta f T_p 2 [f_c + (M-1)\Delta f]}{(f_c + \Delta f)} \stackrel{\Delta f \ll f_c}{\approx} 2\Delta f T_p \end{aligned} \quad (18)$$

depending on the FO and pulse duration T_p . Especially, if $\Delta f = \frac{1}{T_p}$, FDA can radiate the whole airspace within one pulse duration.

- 2) The FDA beam scanning speed depends only on the FO. The larger the angle of the main lobe direction, the faster the beam scanning speed.

Therefore, the auto-scanning property is the essence of FDA antennas.

C. Initial Main Lobe Direction

Since auto-scanning is the most prominent feature of FDA antennas, how to effectively control the initial main lobe direction by designing the transmit weight vector is a problem that must be solved.

Set the transmitted weigh vector

$$\mathbf{w} = [\alpha_\theta(\theta_0) * \alpha_{\Delta f}(\theta_0)]^c \quad (19)$$

and substituting (19) into (6) yields

$$\begin{aligned} y(t) &= \phi(t) e^{j2\pi f_c t} \\ &\quad \cdot \sum_{m=0}^{M-1} \left[e^{-j2\pi f_c \frac{m d \sin \theta_0}{c}} \cdot e^{-j2\pi m \Delta f \frac{m d \sin \theta_0}{c}} \right] \\ &\quad \cdot \left[e^{j2\pi m \Delta f t} e^{j2\pi (f_c + m \Delta f) \frac{m d \sin \theta}{c}} \right] \\ &\approx \phi(t) e^{j2\pi f_c t} \sum_{m=0}^{M-1} e^{j2\pi m \Delta f t} e^{j2\pi (f_c + \Delta f) m d \frac{\sin \theta - \sin \theta_0}{c}}. \end{aligned} \quad (20)$$

Then we can obtain the FDA array factor, i.e., FITB at $t = 0$

$$AF_{\text{FDA}}(0, \theta) = \left| \frac{\sin \left\{ M\pi \left[\frac{(f_c + \Delta f) d (\sin \theta - \sin \theta_0)}{c} \right] \right\}}{\sin \left\{ \pi \left[\frac{(f_c + \Delta f) d (\sin \theta - \sin \theta_0)}{c} \right] \right\}} \right|, \quad (21)$$

and the FITB peak appears at $\theta = \theta_0$. At this point, we have completed the design of the FDA transmitted weight vector.

D. Numerical Simulation

Fig. 2 and Fig. 3 show the FDA array factor (10) and FITB (9) at three different times, respectively. And the beampattern of the phased-array ($\Delta f = 0$) is used as a benchmark. The number of array elements is $M = 16$, reference carrier frequency is $f_c = 10 \text{ GHz}$ and inter-element spacing is $d = \frac{\lambda_0}{2}$ ($d = \frac{c}{2f_c}$ for phased-array). The baseband waveform $\phi(t)$ is a rectangular pulse with pulse duration being $T_p = 5 \mu\text{s}$. In Fig. 2, Fig. 3b and Fig. 3c, the transmitted weight vector is set to $\mathbf{w} = [\alpha_\theta(0^\circ) * \alpha_{\Delta f}(0^\circ)]^c$. In Fig. 3a, the transmitted weight vector is set to $\mathbf{w} = [\alpha_\theta(-20^\circ) * \alpha_{\Delta f}(-20^\circ)]^c$.

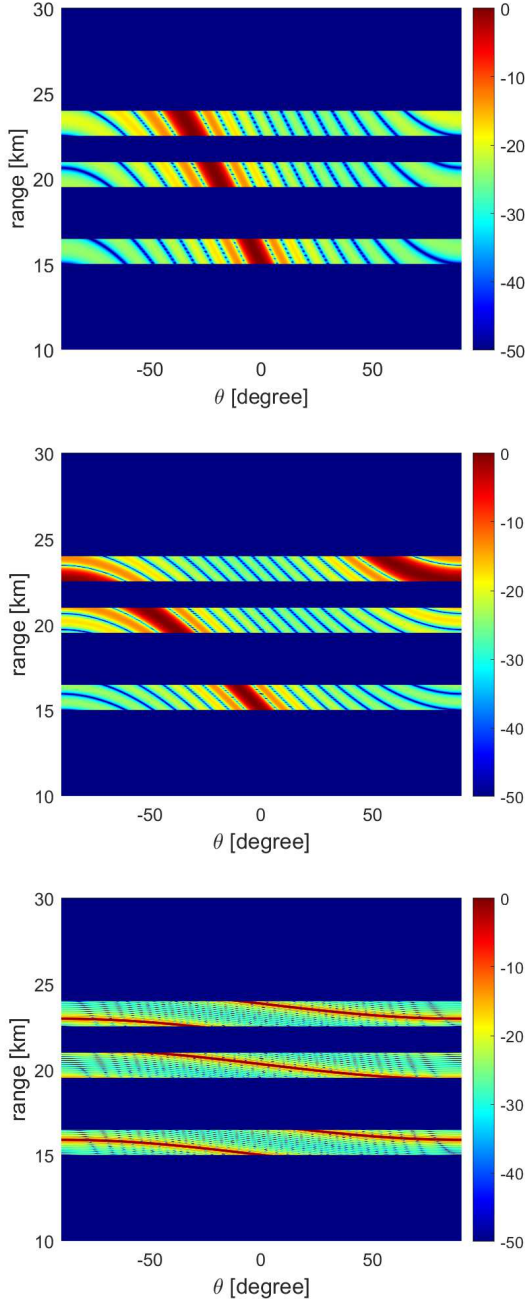


Fig. 2. Illustration of the FDA array factor (10) at the observed instant $t = 50 \mu\text{s}$, $t = 65 \mu\text{s}$ and $t = 75 \mu\text{s}$ in the existing FDA transmit beampattern studies. (a) $\Delta f = 10 \text{ kHz}$. (b) $\Delta f = 20 \text{ kHz}$. (c) $\Delta f = 170 \text{ kHz}$.

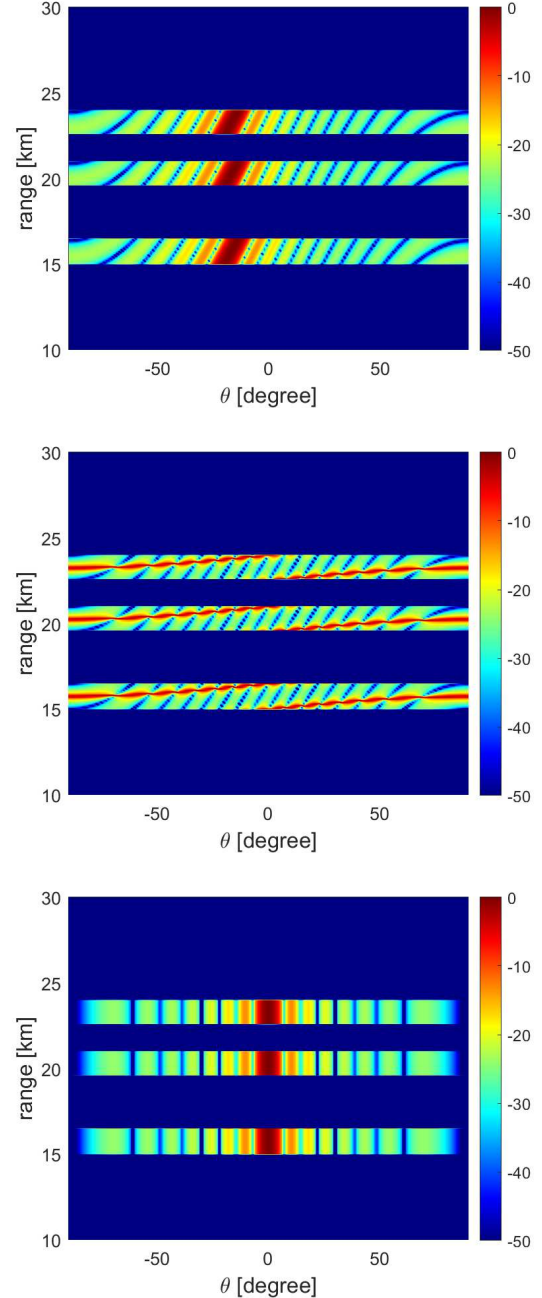


Fig. 3. Illustration of the proposed FITB (9) at the observed instant $t = 50 \mu\text{s}$, $t = 65 \mu\text{s}$ and $t = 75 \mu\text{s}$ with considering the time-range relation. (a) $\Delta f = 10 \text{ kHz}$. (b) $\Delta f = 200 \text{ kHz}$. (c) $\Delta f = 0 \text{ kHz}$.

Comparing Fig. 2 and Fig. 3, we can find that

- Over time, the peak of FITB continues to propagate at speed c in the direction of increased range. And the beam coverage in the pulse duration is always the same. This is completely different from the one shown in Fig. 2. In the existing studies on FDA antennas, the relations between time and range is not considered, resulting in the incorrect analyses for FDA. Besides, many papers refer to this mobility of the transmit beam as the time-variant property, which is obviously wrong. In fact, time-variant and auto-scanning properties are equivalent, it can

be understood from the two perspectives of the pulse duration and beam coverage.

- Small FO produces small beam coverage. At this time, the spatial extent of the FITB within one pulse duration is limited, almost same as conventional phased-array beampattern. The simulation results are consistent with (17).
- For the large FO ($\Delta f = \frac{1}{T_p}$ in Fig. 3b), the beam coverage is the entire observed airspace within one pulse duration. But compared to the small FO case and phased-array, the radiated energy is also dispersed in the entire airspace, which will inevitably lead to a signal-to-noise ratio (SNR) reduction in the receiving stage.
- Observing Fig. 3a and Fig. 3b, we can find that the initial main lobe directions of the FITB are -20° and 0° , respectively. Simulation results are consistent with the parameter design and the analyzed in Section III-C.

IV. THE INFLUENCE OF FO ON FITB

A. Nonlinear FO

Consider the nonlinear FO $\Delta f_m, m = 0, 1, \dots, M-1$, where the FO of each array element is nonlinear [15], [18], [42]. According to the analysis in Section II, the signal arriving at a given far-field point target with range-angle pair (r_t, θ) is

$$y(t) \approx \sum_{m=0}^{M-1} w_m^c \phi\left(t - \frac{r_t}{c}\right) e^{j2\pi(f_c + \Delta f_m)\left(t - \frac{r_t - md \sin \theta}{c}\right)} \quad (22)$$

$$, t \in \left[\frac{r_t}{c}, \frac{r_t}{c} + T_p\right]$$

Then it can be equivalently expressed as

$$r(t') = \phi(t') e^{j2\pi f_c t'} \sum_{m=0}^{M-1} w_m^c e^{j2\pi \Delta f_m t'} e^{j2\pi(f_c + \Delta f_m) \frac{md \sin \theta}{c}} \quad (23)$$

$$, t' \in [0, T_p]$$

And the FITB can be written as

$$AF_{\text{nonlinear-FDA}}(t, \theta) = \alpha_{\text{nonlinear-T}}^T(t) \alpha_{\text{nonlinear-}\Delta f}^T(\theta) \quad (24)$$

where

$$\alpha_{\text{nonlinear-T}}(t) = \begin{bmatrix} e^{j2\pi \Delta f_0 t} & e^{j2\pi \Delta f_1 t} & \dots & e^{j2\pi \Delta f_{M-1} t} \end{bmatrix}^T, \quad (25)$$

$$\alpha_{\text{nonlinear-}\Delta f}^T(\theta) = \begin{bmatrix} e^{j2\pi(f_c + \Delta f_0) \frac{d \sin \theta}{c}} \\ e^{j2\pi(f_c + \Delta f_1) \frac{d \sin \theta}{c}} \\ \dots \\ e^{j2\pi(f_c + \Delta f_{M-1}) \frac{d \sin \theta}{c}} \end{bmatrix}.$$

Note that the FITB with nonlinear FO depends on the time and angle, the same as standard FDA.

B. Time-modulated FO

Consider the time-modulated FO $\Delta f_m = \chi_m(t), m = 0, 1, \dots, M-1, t \in [0, T_p]$, where $\chi_m(t)$ is a function with respect to t [43], [44].

Many papers tries to design $\chi_m(t)$ to obtain the focused FDA array factor (10) [16], [43]–[45], where the signal model is usually written as

$$z(t) \approx \sum_{m=0}^{M-1} \left[w_m^c \phi\left(t - \frac{r_t}{c}\right) \cdot e^{j2\pi[f_c + \chi_m\left(t - \frac{r_t - md \sin \theta}{c}\right)]\left(t - \frac{r_t - md \sin \theta}{c}\right)} \right] \quad (26)$$

In fact, according to the analysis in Section II, the signal arriving at a given far-field point target with range-angle pair (r_t, θ) can be equivalently expressed as

$$r(t') = \sum_{m=0}^{M-1} w_m^c \phi(t') e^{j2\pi[f_c + \chi_m\left(t' + \frac{md \sin \theta}{c}\right)]\left(t' + \frac{md \sin \theta}{c}\right)} \quad (27)$$

$$, t' \in [0, T_p]$$

Then, the FITB can be written as

$$AF_{\text{TM-FDA}}(t, \theta) = \alpha_T^T(\theta) \alpha_{\text{TM-T}}^T(t, \theta) \quad (28)$$

where

$$\alpha_{\text{TM-T}}^T(t, \theta) = \begin{bmatrix} e^{j2\pi \chi_0(t')t'} \\ e^{j2\pi \chi_1\left(t' + \frac{d \sin \theta}{c}\right)\left(t' + \frac{d \sin \theta}{c}\right)} \\ \dots \\ e^{j2\pi \chi_{M-1}\left(t' + \frac{(M-1)d \sin \theta}{c}\right)\left(t' + \frac{(M-1)d \sin \theta}{c}\right)} \end{bmatrix}. \quad (29)$$

We can see that the FITB with time-modulated FO is still time-angle-dependent.

Numerical Simulation: Consider the simulation parameters used in Fig. 2. Fig. 4 shows the FITB of four different FO coding methods. Nonlinear and time-modulated FOs generate irregular intra-pulse beam scanning, but the range-dependent property is certainly not available.

C. FITB Synthesis

Through the above analysis, we can conclude that standard FDA can be simply regarded as a phased-array with time-variant weighting. Next, we give a most intuitive FITB design scheme to explain the relations between FDA and phased-array more clearly.

Suppose the transmitted FDA signal is

$$x(t) = \sum_{m=0}^{M-1} \phi(t) e^{j2\pi(f_c + m\Delta f)t} e^{j2\pi m\varphi(t)}, t \in [0, T_p] \quad (30)$$

where $\varphi(t)$ is a phase function that can be optimized to obtain the desired beampattern. Then, signal arriving at a given far-field point target with range-angle pair (r_t, θ) can be written as

$$y(t) \approx \sum_{m=0}^{M-1} \left[\phi\left(t - \frac{r_t}{c}\right) e^{j2\pi(f_c + m\Delta f)\left(t - \frac{r_t - md \sin \theta}{c}\right)} \cdot e^{j2\pi m\varphi\left(t - \frac{r_t - md \sin \theta}{c}\right)} \right] \quad (31)$$

$$, t \in \left[\frac{r_t}{c}, \frac{r_t}{c} + T_p\right].$$

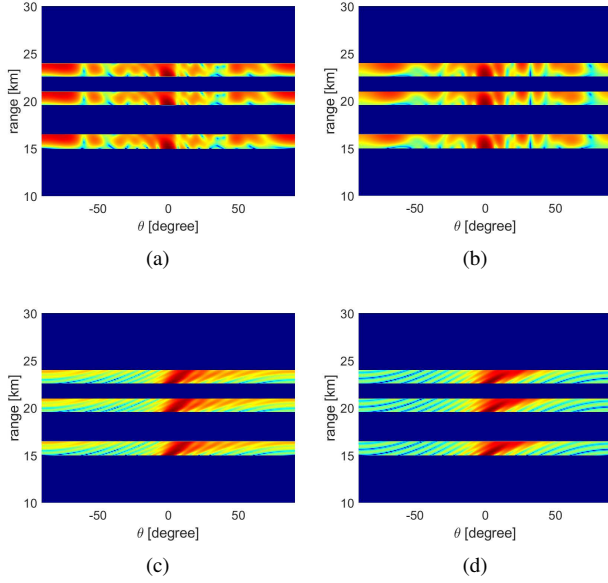


Fig. 4. The FITB of four different FO coding methods at the observed time $t = 50 \mu s$, $t = 60 \mu s$ and $t = 75 \mu s$. (a) Random FO $\Delta f_m = \text{random}_m \Delta f$, $\Delta f = 200 \text{ kHz}$ where $0 \leq \text{random}_m \leq M - 1$ is random code [18]. (b) Costas FO $\Delta f_m = \text{costas}_m \Delta f$, $\Delta f = 200 \text{ kHz}$ where $0 \leq \text{costas}_m \leq M - 1$ is Costas code [42]. (c) Logarithmic FO $\Delta f_m = \ln(m + 1) \Delta f$, $\Delta f = 400 \text{ kHz}$ [15]. (d) Square FO $\Delta f_m = m^2 \Delta f$, $\Delta f = 2 \text{ kHz}$.

Similar to the previous analysis, the FDA array factor or FITB can then be expressed as

$$AF_{\text{FDA}}(t', \theta) = \left| \frac{\sin \left[M\pi \left(\Delta f t' + \varphi(t') + \frac{f_c d \sin \theta}{c} + \frac{\Delta f d \sin \theta}{c} \right) \right]}{\sin \left[\pi \left(\Delta f t' + \varphi(t') + \frac{f_c d \sin \theta}{c} + \frac{\Delta f d \sin \theta}{c} \right) \right]} \right| \quad (32)$$

$, t' \in [0, T_p].$

It has peaks at the locations satisfying

$$\Delta f t' + \varphi(t') + \frac{f_c d \sin \theta}{c} + \frac{\Delta f d \sin \theta}{c} = k, \quad k \in \mathbb{Z}. \quad (33)$$

Note that the beam scanning for different observed airspace can be realized by designing $\varphi(t')$.

For example, if we expect the FDA beam steer to the area $\theta \in [\theta_1, \theta_2]$ at $t' \in [0, T_1]$ and the area $\theta \in [\theta_3, \theta_4]$ at $t' \in [T_2, T_p]$, with no main lobe during other periods of the pulse

duration. To this end, we can set

$$\varphi(t') = \begin{cases} \begin{cases} -\Delta f t' - \frac{(f_c + \Delta f) d \sin \left(\frac{\theta_2 - \theta_1}{T_1} t' + \theta_1 \right)}{c} \\ t' \in [0, T_1] \\ \theta \in [\theta_1, \theta_2] \end{cases} \\ \frac{1}{M} - \Delta f t' - \frac{(f_c + \Delta f) d \sin[\mu(t')]}{c}, & \text{other} \\ \begin{cases} -\Delta f t' - \frac{(f_c + \Delta f) d}{c} \\ \cdot \sin \left[\frac{\theta_4 - \theta_3}{T_p - T_2} t' + \theta_3 - \frac{T_2(\theta_4 - \theta_3)}{T_p - T_2} \right] \\ t' \in [T_2, T_p] \\ \theta \in [\theta_3, \theta_4] \end{cases} \end{cases} \quad (34)$$

where $\mu(t')$ is a function with respect to t' . Substituting (34) into (33), and it can be noted that we have completed the above-described beam design tasks.

From another viewpoint, if we substitute (34) into (30), we have

$$x(t) \approx \begin{cases} \begin{cases} \phi(t) \sum_{m=0}^{M-1} e^{-j2\pi m \frac{(f_c + \Delta f) d \sin \left(\frac{\theta_2 - \theta_1}{T_1} t + \theta_1 \right)}{c}} \\ t \in [0, T_1] \\ \theta \in [\theta_1, \theta_2] \end{cases} \\ [0, & \text{other} \\ \begin{cases} \phi(t) \sum_{m=0}^{M-1} e^{-j2\pi m \frac{(f_c + \Delta f) d \sin \left[\frac{\theta_4 - \theta_3}{T_p - T_2} t + \theta_3 - \frac{T_2(\theta_4 - \theta_3)}{T_p - T_2} \right]}{c}} \\ t \in [T_2, T_p] \\ \theta \in [\theta_3, \theta_4] \end{cases} \end{cases} \quad (35)$$

In such case, the FDA configuration is completely equivalent to a phased-array with the carrier frequency being $f_c + \Delta f$.

V. FDA INTEGRAL TRANSMIT BEAMPATTERN

Since the FITB derived from the FDA array factor is time-variant, we can integrate it over the pulse duration to eliminate the influence of time on the beampattern. Then, we can get the FDA integral transmit beampattern (FGTB).

Define FGTB as:

$$\begin{aligned} P_{\text{FGTB}}(\mathbf{w}, \Delta f, \theta) &= \frac{1}{T_p} \int_0^{T_p} r(t) r^c(t) dt \\ &= \frac{1}{T_p} \int_0^{T_p} \left\{ \begin{array}{l} \phi(t) \phi^H(t) [\mathbf{w}^c * \alpha_{\text{FDA}, \Delta f}(\theta)]^T \\ \alpha_T(t) \alpha_T^H(t) [\mathbf{w}^c * \alpha_{\text{FDA}, \Delta f}(\theta)]^c \end{array} \right\} dt \\ &= [\mathbf{w}^c * \alpha_{\text{FDA}, \Delta f}(\theta)]^T \frac{1}{T_p} \int_0^{T_p} \phi(t) \alpha_T(t) \alpha_T^H(t) \phi^H(t) dt \\ &= [\mathbf{w}^c * \alpha_{\text{FDA}, \Delta f}(\theta)]^c \\ &= \frac{1}{T_p} \text{tr} \left\{ \mathbf{R}_{\text{FDA}} [\mathbf{w}^c * \alpha_{\text{FDA}, \Delta f}(\theta)]^c [\mathbf{w}^c * \alpha_{\text{FDA}, \Delta f}(\theta)]^T \right\} \end{aligned} \quad (36)$$

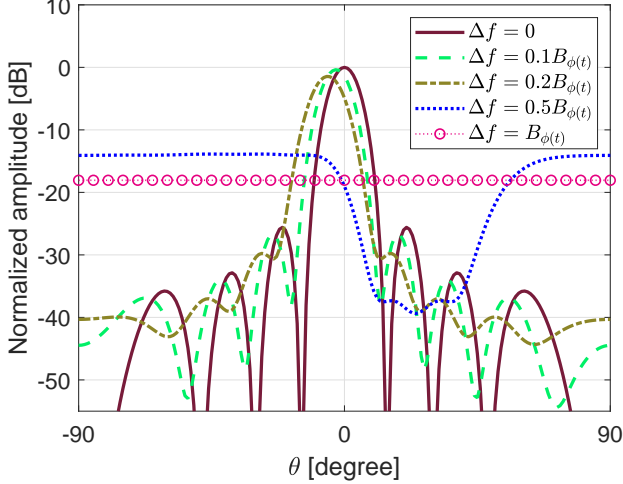


Fig. 5. FDA integral transmit beampattern.

where $\mathbf{R}_{\text{FDA}} = \int_0^{T_p} \phi(t) \alpha_T(t) \alpha_T^H(t) \phi^H(t) dt \in \mathbb{C}^{M \times M}$ can be regarded as the covariance matrix of the FDA transmitted signal and $\text{tr}\{\mathbf{Q}\}$ represents the trace of the matrix \mathbf{Q} .

- For $M\Delta f \ll B_{\phi(t)}$, we have $\mathbf{R}_{\text{FDA}} \approx \mathbf{1}$. FGTB can be approximately written as $P_{\text{FGTB}}(\mathbf{w}, \Delta f, \theta) \approx \frac{1}{T_p} |\mathbf{w}^H \alpha_{\text{FDA}, \Delta f}(\theta)|^2$ and simplified to the conventional phased-array beampattern.
- If $\Delta f \geq B_{\phi(t)}$, then $\mathbf{R}_{\text{FDA}} \approx \mathbf{I}$ with \mathbf{I} being identity matrix. FGTB can be approximately written as $P_{\text{FGTB}}(\mathbf{w}, \Delta f, \theta) \approx \frac{1}{T_p} \|\mathbf{w}\|^2$ with $\|\cdot\|$ denoting l_2 norm. FGTB is omnidirectional, corresponding to the orthogonal MIMO beampattern.

Numerical Simulation: The number of array elements is $M = 16$ and uniformly weighted, reference carrier frequency is $f_c = 10 \text{ GHz}$. The baseband waveform is a rectangular pulse signal with unit energy and pulse duration is $T_p = 10 \text{ ns}$. The simulation result of FGTB is shown in the Fig. 5.

Note that the FO increases, the coherent gain decreases and the beam main lobe expands. For $\Delta f = B_{\phi(t)}$, the transmitted waveforms are orthogonal, resulting in omnidirectional energy radiation, and coherent gain does not exist.

This can also be explained from the perspective of beam scanning (as analyzed in (18)). For small FO, the beam coverage is negligible during the pulse duration, so the FGTB is similar to the conventional phased-array beampattern. And when $\Delta f = B_{\phi(t)}$, the FDA can scan the observed airspace from 0° to 180° within one pulse duration, which corresponds to an omnidirectional FGTB.

A. FO Effect

The existing FDA literature [14], [31], [33] ignores the vector $\alpha_{\Delta f}(\theta)$ in signal model based on the following assumption

$$2\pi\Delta f \frac{m^2 d \sin \theta}{c} \leq \frac{\pi}{4}, \quad m = 0, 1, \dots, M-1 \quad (37)$$

Then we have

$$\Delta f \leq \frac{f_c}{4M^2 - M} \quad (38)$$

We call the vector $\alpha_{\Delta f}(\theta)$ in the beampattern as the FO effect.

Combined with the narrowband assumption (4), in the signal model (6), FO needs to satisfy

$$\frac{MB_{\phi(t)} - f_c}{2M} \ll \Delta f \leq \frac{f_c}{4M^2 - M}. \quad (39)$$

Therefore, the FO effect must be considered for scenarios with large array apertures and high range resolution requirements. In particular, For FDA-MIMO [29], [46], its configuration requires each element to transmit the baseband waveforms with non-overlapping spectra, i.e., $\Delta f \geq B_{\phi(t)}$. In this case, FO will not meet the requirements of (39), and the FO effect must be considered.

B. FGTB Synthesis Based On Waveform Optimization

In this subsection, we mainly consider the relations between the FGTB and the co-located MIMO transmit beampattern.

The transmitted co-located MIMO signal can be written as [47], [48]:

$$x(t) = \sum_{m=0}^{M-1} w_m^c \phi_m(t) e^{j2\pi f_c t}, \quad t \in [0, T_p] \quad (40)$$

where $\phi_m(t)$ denotes the baseband complex waveform transmitted by the m th element. Then, the synthesized signals arriving at a given far-field point target with range-angle pair (r_t, θ) is

$$y(t) \approx \sum_{m=0}^{M-1} w_m^c \phi_m\left(t - \frac{r_t}{c}\right) e^{j2\pi f_c \left(t - \frac{r_t - m d \sin \theta}{c}\right)}, \quad t \in \left[\frac{r_t}{c}, \frac{r_t}{c} + T_p\right] \quad (41)$$

Then, it can be simplified to

$$r(t') = \sum_{m=0}^{M-1} w_m^c \phi_m(t') e^{j\frac{2\pi}{\lambda} m d \sin \theta}, \quad t' \in [0, T_p] \quad (42)$$

And we can obtain the co-located MIMO transmit beampattern [20]

$$P_{\text{MIMO}}(\mathbf{w}, \theta) = \text{tr} \left\{ \mathbf{R}_{\text{MIMO}}[\mathbf{w}^c * \alpha_T(\theta)]^c [\mathbf{w}^c * \alpha_T(\theta)]^T \right\} \quad (43)$$

where $\mathbf{R}_{\text{MIMO}} = \int_0^{T_p} \phi(t) \phi^H(t) dt \in \mathbb{C}^{M \times M}$ can be treated as the covariance matrix of the transmitted MIMO signal with $\phi(t) = [\phi_0(t) \ \phi_1(t) \ \dots \ \phi_{M-1}(t)]^T$ being the transmitted waveform vector.

Comparing (36) and (43), we can find that the beampattern difference between FDA and co-located MIMO only exists in the FO effect analyzed in Section V-A.

If the FO effect on the FGTB can be neglected, the FGBT synthesis problem based on waveform optimization can be completely equivalent to the beampattern design of co-located MIMO, and a large number of papers have been published about MIMO beampattern design [49]–[52]. However, it is very difficult to describe the influence of the FO effect on FGTB analytically. Therefore, the influence is verified by numerical simulations.

Numerical Simulation: The number of array elements is $M = 16$, reference carrier frequency is $f_c = 10 \text{ GHz}$.

- For co-located MIMO, a chirp signal is used and a uniform FO is added as the transmitted waveform, where bandwidth of the chirp signal belongs to $B_{s_m(t)} \in [100, 400] \text{ MHz}$. Then the waveform transmitted by the m th element can be written as

$$\begin{aligned} \phi_m(t) &= s_m(t) e^{j2\pi m \Delta f t}, \\ B_{s_m(t)} &= \left(100 + \frac{40m}{M}\right) \text{MHz} \quad (44) \\ &, m = 0, 1, \dots, M-1 \end{aligned}$$

with $s_m(t)$ being the m th chirp signal. And the co-located MIMO beampattern is calculated based on (44).

- For FDA, the baseband waveform transmitted by the m th array is

$$\begin{aligned} \phi_m(t) &= s_m(t), \quad B_{s_m(t)} = \left(100 + \frac{40m}{M}\right) \text{MHz} \\ &, m = 0, 1, \dots, M-1 \quad (45) \end{aligned}$$

with $s_m(t)$ being the m th chirp signal. The FGTB is calculated based on (36).

Fig. 6 shows the simulation results of FGTB and co-located MIMO beampattern where $B = 100 \text{ MHz}$. It can be seen that there is no obvious difference between FGTB which considers the FO effect and the co-located MIMO beampattern. Therefore, we can conclude that the desired waveform of FGTB synthesis can be equivalent to waveforms designed by the corresponding co-located MIMO beampattern.

Suppose the desired beampattern is $D(\theta)$, and the m th element transmitted waveform synthesized by the co-located MIMO design method is $d_m(t)$. Then, for FDA, the beampattern $D(\theta)$ can also be obtained by setting the transmitted waveform of the m th array element to $\frac{d_m(t)}{e^{j2\pi m \Delta f t}}$ where FO satisfies the constraint of (39).

VI. CONCLUSION

In this paper, we reinterpreted the characteristics of FDA transmit beampattern and reformulated the FDA transmitted signal model with the consideration of FDA time-range relations. Two FDA transmit beampattern models are formulated, namely, instantaneous transmit beampattern and integral transmit beampattern. The corresponding beampattern design schemes also are given. Both theoretical analysis and simulation results prove that the FDA antenna provides auto-scanning capability, but the range-dependence is not available in fact. We also justified that the frequency offset effect is the only difference that between the FDA integral transmit beampattern and the co-located MIMO beampattern. This paper is meaningful in understanding FDA range-time relations, which provides a reference to design efficient FDA receiver. More importantly, we should exploit the FDA time-variance for enhanced system performance, rather than removing the time-variance for focused beampattern.

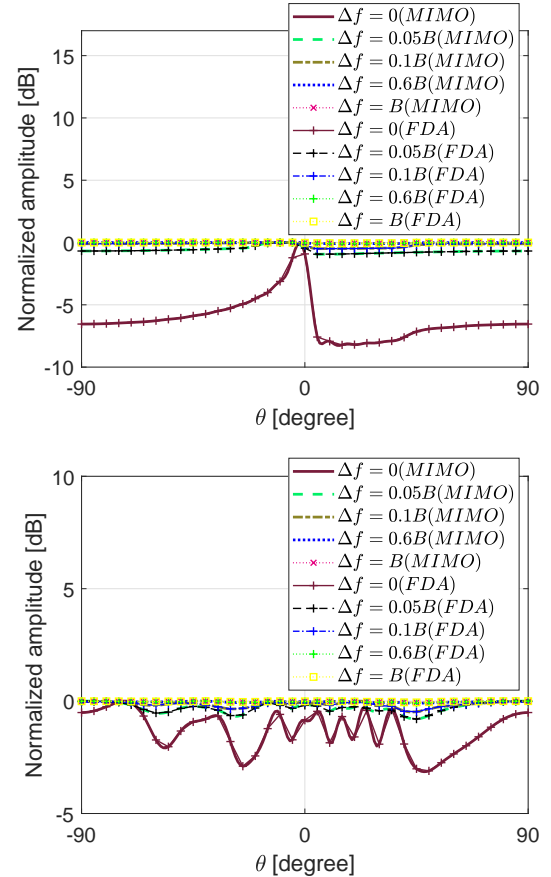


Fig. 6. Comparison of the FGTB and co-located MIMO transmit beampattern, with (a) uniform transmit weight $\mathbf{w} = \mathbf{1}_M$ with $\mathbf{1}_M$ being $M \times 1$ vector of ones; (b) random transmit weight $w_m = e^{j2\pi c_m m}$, $m = 1, \dots, M-1$ with $0 \leq c_m \leq 1$ being random number.

REFERENCES

- [1] P. Antonik, M. C. Wicks, H. D. Griffiths, and C. J. Baker, "Frequency diverse array radars," in *2006 IEEE Conference on Radar*. IEEE, 2006, pp. 3–pp.
- [2] —, "Multi-mission multi-mode waveform diversity," in *2006 IEEE Conference on Radar*. IEEE, 2006, pp. 3–pp.
- [3] M. C. Wicks and P. Antonik, "Method and apparatus for a frequency diverse array," Mar. 31 2009, uS Patent 7,511,665.
- [4] —, "Frequency diverse array with independent modulation of frequency, amplitude, and phase," Jan. 15 2008, uS Patent 7,319,427.
- [5] M. Secmen, S. Demir, A. Hizal, and T. Eker, "Frequency diverse array antenna with periodic time modulated pattern in range and angle," in *2007 IEEE Radar Conference*. IEEE, 2007, pp. 427–430.
- [6] J. Huang, K.-F. Tong, and C. Baker, "Frequency diverse array with beam scanning feature," in *2008 IEEE Antennas and Propagation Society International Symposium*. IEEE, 2008, pp. 1–4.
- [7] P. Sammartino and C. Baker, "The frequency diverse bistatic system," in *2009 International Waveform Diversity and Design Conference*. IEEE, 2009, pp. 155–159.
- [8] —, "Developments in the frequency diverse bistatic system," in *2009 IEEE Radar Conference*. IEEE, 2009, pp. 1–5.
- [9] C. Cetintepe and S. Demir, "Multipath characteristics of frequency diverse arrays over a ground plane," *IEEE Transactions on Antennas and Propagation*, vol. 62, no. 7, pp. 3567–3574, 2014.
- [10] W.-Q. Wang, "Cognitive frequency diverse array radar with situational awareness," *IET Radar, Sonar & Navigation*, vol. 10, no. 2, pp. 359–369, 2016.
- [11] —, "Moving-target tracking by cognitive rf stealth radar using frequency diverse array antenna," *IEEE Transactions on Geoscience and Remote Sensing*, vol. 54, no. 7, pp. 3764–3773, 2016.

- [12] —, “Potential transmit beamforming schemes for active lpi radars,” *IEEE Aerospace and Electronic Systems Magazine*, vol. 32, no. 5, pp. 46–52, 2017.
- [13] —, “Retrodirective frequency diverse array focusing for wireless information and power transfer,” *IEEE Journal on Selected Areas in Communications*, vol. 37, no. 1, pp. 61–73, 2018.
- [14] W. Q. Wang, “Overview of frequency diverse array in radar and navigation applications,” *IET Radar Sonar & Navigation*, vol. 10, no. 6, pp. 1001–1012, 2016.
- [15] W. Khan, I. M. Qureshi, and S. Saeed, “Frequency diverse array radar with logarithmically increasing frequency offset,” *IEEE antennas and wireless propagation letters*, vol. 14, pp. 499–502, 2014.
- [16] W. Khan and I. M. Qureshi, “Frequency diverse array radar with time-dependent frequency offset,” *IEEE Antennas and Wireless Propagation Letters*, vol. 13, pp. 758–761, 2014.
- [17] W. Khan, I. M. Qureshi, A. Basit, and W. Khan, “Range-bins-based mimo frequency diverse array radar with logarithmic frequency offset,” *IEEE Antennas and Wireless Propagation Letters*, vol. 15, pp. 885–888, 2015.
- [18] Y. Liu, R. Hang, L. Wang, and A. Nehorai, “The random frequency diverse array: A new antenna structure for uncoupled direction-range indication in active sensing,” *IEEE Journal of Selected Topics in Signal Processing*, vol. 11, no. 2, pp. 295–308, 2017.
- [19] J. Xiong, W.-Q. Wang, H. Shao, and H. Chen, “Frequency diverse array transmit beampattern optimization with genetic algorithm,” *IEEE Antennas and Wireless Propagation Letters*, vol. 16, pp. 469–472, 2016.
- [20] J. Li and P. Stoica, “Mimo radar with colocated antennas,” *IEEE Signal Processing Magazine*, vol. 24, no. 5, pp. 106–114, 2007.
- [21] A. M. Haimovich, R. S. Blum, and L. J. Cimini, “Mimo radar with widely separated antennas,” *IEEE Signal Processing Magazine*, vol. 25, no. 1, pp. 116–129, 2007.
- [22] P. F. Sannmartino, C. J. Baker, and H. D. Griffiths, “Frequency diverse mimo techniques for radar,” *IEEE Transactions on Aerospace and Electronic Systems*, vol. 49, no. 1, pp. 201–222, 2013.
- [23] A. Basit, W.-Q. Wang, S. Wali, and S. Y. Nusenu, “Transmit beamspace design for fda-mimo radar with alternating direction method of multipliers,” *Signal Processing*, vol. 180, p. 107832, 2021.
- [24] W. Q. Wang and H. Shao, “Range-angle localization of targets by a double-pulse frequency diverse array radar,” *IEEE Journal of Selected Topics in Signal Processing*, vol. 8, no. 1, pp. 106–114, 2014.
- [25] W. Q. Wang and H. C. So, “Transmit subaperturing for range and angle estimation in frequency diverse array radar,” *IEEE Transactions on Signal Processing*, vol. 62, no. 8, pp. 2000–2011, 2014.
- [26] W. Q. Wang, “Subarray-based frequency diverse array radar for target range-angle estimation,” *Aerospace & Electronic Systems IEEE Transactions on*, vol. 50, no. 4, pp. 3057–3067, 2014.
- [27] A. Basit, W. Q. Wang, S. Y. Nusenu, and S. Zhang, “Range-angle-dependent beampattern synthesis with null depth control for joint radar communication,” *IEEE Antennas and Wireless Propagation Letters*, vol. 18, no. 9, pp. 1741–1745, 2019.
- [28] J. Xu, G. Liao, S. Zhu, and H. C. So, “Deceptive jamming suppression with frequency diverse mimo radar,” *Signal Processing*, vol. 113, pp. 9–17, 2015.
- [29] J. Xu, S. Zhu, and G. Liao, “Range ambiguous clutter suppression for airborne fda-stap radar,” *IEEE Journal of Selected Topics in Signal Processing*, vol. 9, no. 8, pp. 1620–1631, 2015.
- [30] J. Xiong, W. Q. Wang, C. Cui, and K. Gao, “Cognitive fda-mimo radar for lpi transmit beamforming,” *IET Radar Sonar & Navigation*, vol. 11, no. 10, pp. 1574–1580, 2017.
- [31] J. Hu, S. Yan, F. Shu, J. Wang, J. Li, and Y. Zhang, “Artificial-noise-aided secure transmission with directional modulation based on random frequency diverse arrays,” *IEEE Access*, vol. 5, pp. 1658–1667, 2017.
- [32] Y. Xu and K.-M. Luk, “Enhanced transmit–receive beamforming for frequency diverse array,” *IEEE Transactions on Antennas and Propagation*, vol. 68, no. 7, pp. 5344–5352, 2020.
- [33] R. Gui, W.-Q. Wang, C. Cui, and H. C. So, “Coherent pulsed-fda radar receiver design with time-variance consideration: Sinr and crb analysis,” *IEEE Transactions on Signal Processing*, vol. 66, no. 1, pp. 200–214, 2018.
- [34] A.-M. Yao, W. Wu, and D.-G. Fang, “Frequency diverse array antenna using time-modulated optimized frequency offset to obtain time-invariant spatial fine focusing beampattern,” *IEEE Transactions on Antennas and Propagation*, vol. 64, no. 10, pp. 4434–4446, 2016.
- [35] W.-Q. Wang, “Range-angle dependent transmit beampattern synthesis for linear frequency diverse arrays,” *IEEE transactions on antennas and propagation*, vol. 61, no. 8, pp. 4073–4081, 2013.
- [36] Y. Xu, X. Shi, J. Xu, and P. Li, “Range-angle-dependent beamforming of pulsed frequency diverse array,” *IEEE Transactions on Antennas and Propagation*, vol. 63, no. 7, pp. 3262–3267, 2015.
- [37] H. Wang, G. Liao, J. Xu, and S. Zhu, “Transmit beampattern design for coherent fda by piecewise lfm waveform,” *Signal processing*, vol. 161, pp. 14–24, 2019.
- [38] —, “Space-time matched filter design for interference suppression in coherent frequency diverse array,” *IET Signal Processing*, vol. 14, no. 3, pp. 175–181, 2020.
- [39] L. Lan, J. Xu, G. Liao, Y. Zhang, F. Fioranelli, and H. C. So, “Suppression of mainbeam deceptive jammer with fda-mimo radar,” *IEEE Transactions on Vehicular Technology*, vol. 69, no. 10, pp. 11 584–11 598, 2020.
- [40] A. M. Yao, W. Wu, and D. G. Fang, “Solutions of time-invariant spatial focusing for multi-targets using time modulated frequency diverse antenna arrays,” *IEEE Transactions on Antennas and Propagation*, vol. 65, no. 2, pp. 552–566, 2017.
- [41] P. Urone and R. Hinrichs, “College physics,” 1998.
- [42] Z. Wang, W.-Q. Wang, and H. Shao, “Range-azimuth decouple beamforming for frequency diverse array with costas-sequence modulated frequency offsets,” *EURASIP Journal on Advances in Signal Processing*, vol. 2016, no. 1, pp. 1–9, 2016.
- [43] A.-M. Yao, W. Wu, and D.-G. Fang, “Solutions of time-invariant spatial focusing for multi-targets using time modulated frequency diverse antenna arrays,” *IEEE Transactions on Antennas and Propagation*, vol. 65, no. 2, pp. 552–566, 2016.
- [44] A.-M. Yao, P. Rocca, W. Wu, A. Massa, and D.-G. Fang, “Synthesis of time-modulated frequency diverse arrays for short-range multi-focusing,” *IEEE Journal of Selected Topics in Signal Processing*, vol. 11, no. 2, pp. 282–294, 2016.
- [45] H. Shao, X. Li, W.-Q. Wang, J. Xiong, and H. Chen, “Time-invariant transmit beampattern synthesis via weight design for fda radar,” in *2016 IEEE Radar Conference (RadarConf)*. IEEE, 2016, pp. 1–4.
- [46] P. F. Sannmartino, C. J. Baker, and H. D. Griffiths, “Frequency diverse mimo techniques for radar,” *IEEE Transactions on Aerospace and Electronic Systems*, vol. 49, no. 1, pp. 201–222, 2013.
- [47] G. Hua and S. S. Abeysekera, “Colocated mimo radar transmit beamforming using orthogonal waveforms,” in *2012 IEEE International Conference on Acoustics, Speech and Signal Processing (ICASSP)*. IEEE, 2012, pp. 2453–2456.
- [48] Z. Cheng, B. Liao, Z. He, J. Li, and J. Xie, “Joint design of the transmit and receive beamforming in mimo radar systems,” *IEEE Transactions on Vehicular Technology*, vol. 68, no. 8, pp. 7919–7930, 2019.
- [49] P. Stoica, J. Li, and Y. Xie, “On probing signal design for mimo radar,” *IEEE Transactions on Signal Processing*, vol. 55, no. 8, pp. 4151–4161, 2007.
- [50] S. Ahmed and M.-S. Alouini, “Mimo radar transmit beampattern design without synthesising the covariance matrix,” *IEEE Transactions on Signal Processing*, vol. 62, no. 9, pp. 2278–2289, 2014.
- [51] X. Zhang, Z. He, L. Rayman-Bacchus, and J. Yan, “Mimo radar transmit beampattern matching design,” *IEEE Transactions on Signal Processing*, vol. 63, no. 8, pp. 2049–2056, 2015.
- [52] A. Aubry, A. De Maio, and Y. Huang, “Mimo radar beampattern design via psl/isl optimization,” *IEEE Transactions on Signal Processing*, vol. 64, no. 15, pp. 3955–3967, 2016.